Analysis of Laser and Detector Placement in Incoherent MIMO Multimode Fiber Systems

Kumar Appaiah, Sagi Zisman, Abhik Kumar Das, Sriram Vishwanath, and Seth R. Bank

***Abstract*—Conventional large-core multimode fibers (MMFs) are preferred for use in short to medium haul optical fiber links, owing to their tolerance to misalignment and low deployment costs; however, data rates through MMFs are limited by modal dispersion. Digital signal processing with multiple-input multiple-output (MIMO) techniques has offered promising solutions to overcome the dispersion limitations of MMFs, but the impact of the geometry of laser and detector arrays on the achievable data rate is not established. To this end, we use a field-propagation-based model to gauge the impact the geometry of lasers and detectors can have on the achievable ergodic and outage rates of incoherent MIMO-MMF links. Laser and detector array geometries were investigated using a grid-based method to optimize the positions of lasers and detectors for a 1 km MIMO-MMF link. Simulations reveal that systems with appropriately designed laser/detector geometries could improve the achievable rate over the fiber by more than 200% over random laser/detector arrays. The grid-based search technique, however, is limited due to high computational requirements for fine grids. As an alternative, we developed a suboptimal "greedy" selection approach to design detector geometries, which produces detector geometries that attain more than 90% of the rate obtained with an exhaustive search, while requiring less than 0.2% of the computation. The low computation requirements and high performance of the greedy selection approach also motivate the use of dynamically reconfigurable detector arrays to achieve high data rates with reduced signal processing complexity. Methods are also presented for clustering detector elements to obtain more consolidated segmented detectors with better fill factors, while still offering significant data rate benefits. The achievable ergodic rate using these systems is verified to be close to the link's ergodic capacity.**

***Index Terms*—Fiber optics; Multiplexing; OFDM; Optical fiber communication.**

I. Introduction

Optical fibers form an integral part of current networking architectures due to their ability to support extremely high data rates. Single-mode fibers (SMFs) have long been the choice for high-speed, long-distance optical links owing to their low dispersion and large bandwidth. However, these improvements come with additional complexity in alignment and packaging, making SMFs expensive and less attractive for small to medium sized networks. On the other hand, multimode fibers (MMFs) have relaxed alignment tolerances and lower deployment costs owing to their large core diameter, but modal dispersion limits their bandwidth-length product significantly [1]. While this is perhaps less of an issue in short reach networks, it is, nonetheless, desirable to increase achievable data rates over MMFs. Several recent advances in dispersion compensation techniques have enabled modest increases in data rates through MMFs [2,3]. To support even greater speeds, it is necessary to utilize the fundamental propagation characteristics of MMFs, which is the goal of techniques such as mode-division multiplexing and multiple-input multiple-output (MIMO). In the case of MIMO, it is essential to consider the geometry of the multiple sources and detectors that can take advantage of the modal diversity inherent in MMFs. Here, we develop a framework for analyzing and designing arrays of multiple lasers and detectors for MIMO-MMF links, and study the impact their geometry can have on the data rates achievable over MMF links via simulation.

The primary motivation for this work stems from antenna placement concepts in wireless MIMO systems. In wireless MIMO systems, carefully designed antenna placement ensures the independence of channel coefficients, which enhances the channel's reliability and multiplexing capabilities [4]. The conditions for obtaining the maximum diversity in a wireless link are met by separating antennas of a wireless system with appropriate spacing, a condition that is easily satisfied, given the unguided nature of the wireless propagation medium. The analogous problem in the MIMO-MMF context is to determine optimal placement strategies for lasers and detectors, since this would enable effective separation of signals across various orthogonal modes of the MMF. This problem is complicated by the fact that the modal diversity in MMFs stems from orthogonal modes that occupy the same spatial region of the guiding medium (the MMF core). This makes it difficult to draw conclusions regarding the optimal signal launch and detection geometries that maximize data rates in MIMO-MMF links. To this end, we adopt the field propagation analysis technique developed in [5] and apply it to the MIMO-MMF channel to study the role of laser and detector placement on link performance. Our simulations indicate that optimized placement strategies yield 2–3

Manuscript received August 1, 2013; revised December 28, 2013; accepted January 31, 2014; published March 6, 2014 (Doc. ID 195043).

The authors are with the Department of Electrical and Computer Engineering, The University of Texas at Austin, Austin, Texas 78712, USA (e-mail: kumar.a@utexas.edu).

http://dx.doi.org/10.1364/JOCN.6.000371

times the achievable ergodic rate of arbitrary placements, due to improved modal diversity.

In recent years, the use of MIMO and signal processing for MMF links has received considerable attention. The utility of such techniques was first demonstrated by Stuart [6]. Since then, optical MIMO techniques have been studied with both coherent [7] and incoherent [8,9] detection. In addition, mode-group diversity multiplexing for fiber links has been used as a multiplexing method for improving data rates within dispersion limits [10]. MIMO concepts have also been applied to few-mode and multicore fibers [11–16] and SMFs (as polarization MIMO) [17,18] to significantly improve data rates; however, these require specialty fiber media that are engineered to take advantage of these gains. In our work, we restrict our focus to conventional MMFs, whose core radii range from 50 to 62.5 μm. The utility of multiplexing techniques over conventional MMFs has been well established in the past [6,8,10,19–21], although a fundamental analytical framework for MIMO communication over MMFs remains absent. The use of offset coupling, namely the launching and detection of signals in MMFs with a radial offset to the fiber axis, has been shown to be a useful technique to improve MMF data rates [22–24]. Offset coupling at the transmitter and receiver has been established to be an effective means to realize effective multiplexing through MMFs [25–27]. The feasibility of using multiple lasers and detectors to improve data rate performance was analyzed in [19], where a power diffusion approach was employed to quantify the effectiveness of sending multiple parallel streams of data through the fiber using mode groups. However, the impact of device placement geometry on the achievable data rates over MIMO-MMF has not been studied.

In this paper, we utilize a field propagation analysis technique [5], and develop a framework to optimize laser and detector placement by maximizing the achievable (information theoretic) rate of MIMO-MMF links. Simulations using this model revealed that laser and detector geometry on the input and output facets of the fiber affect the achievable rate, and this was used to determine configurations of lasers and detectors that achieve the largest information theoretic data rate using a grid-based search. For fine grids, exhaustively searching for these configurations becomes computationally expensive, and we introduce a submodular, "greedy" search that produces detector array geometries for fixed laser arrays that attain in excess of 90% of the rate achievable by the optimal configuration, while requiring far fewer computations (more than 99% reduction). The greedy search approach aggressively seeks to place detectors where the dominant modes' power is received. While the efficient greedy search technique is useful for developing static detector arrays, a small number of computations can also be used to enable dynamically reconfigurable detector arrays for reduced complexity signal processing [28].

The paper is organized as follows: Section II describes the physical model of the fiber channel and its statistical nature. Section III outlines the formulation of a MIMO system matrix for each channel realization, develops the input–output model, and discusses the metrics for determining the quality of the channel for given device configurations. Section IV discusses the techniques for efficient optimization of source and detector array geometries. Section V describes the simulation results for select configurations and shows that a "good" configuration can be found under certain constraints. Clustering the arrays to consolidate them into segmented detectors having better fill factors is also discussed. Finally, Section VI concludes the paper.

II. Multimode Fiber Model

To model signal propagation through a MMF, we build upon tools developed by Shemirani *et al.* [5] to arrive at MIMO and signal processing metrics that can be optimized. Other models that can potentially be used to model propagation in MMFs include the diffusion power flow approach, which treats modal coupling as a continuous power diffusion equation along the length of the fiber [29]. This diffusion model assumes that coupling only occurs between nearest neighbor modes and accounts for a power loss mechanism using a mode-dependent parameter that can be measured experimentally [30]. While this approach is suitable for modeling modal coupling, it does not account for other factors, including the polarization of the electric field and changes to the polarization by fiber nonidealities and birefringence. In contrast to the diffusion-based model, our approach treats modal coupling in a perturbation framework, where the perturbing effect is due to bending and twisting of the fiber, thus making it suitable for analyzing MIMO transmission over real MMFs.

We restrict our consideration to intensity modulation and direct-detection-based links. The use of MIMO over long fiber links requires coherent detection to distinguish between the signal contents of various transmit modes. However, over short links, of up to about 1 km, coupling across mode groups is small, and thus the impact of nonlinear mixing of modes at the detector does not significantly affect MIMO performance [26,31].

Figure 1 describes the system setting under which the evaluation is considered. For an $N_T \times N_R$ system that has N_T transmit inputs into the fiber, the laser is split into $2N_T$ arms. These are modulated with transmit signals using an external modulator, and paired up to be superimposed on two different polarizations before being launched into the fiber. In a similar vein, during the decoding process, each output is first split into two polarizations, and an incoherent decoding process, similar to the one implemented in [9,10,32] is used to recover data. In effect, the implementation is a $2N_T \times 2N_R$ MIMO system, where the factor of 2 arises from polarization multiplexing. Such a MIMO system implementation involves the use of pigtail fibers to launch and detect signals with mode filtering [33], or use of a free-space coupling approach [34–36]. For convenience of representation, in this paper, we refer to each launch and detect system as a single laser and detector, respectively, with the implicit understanding that

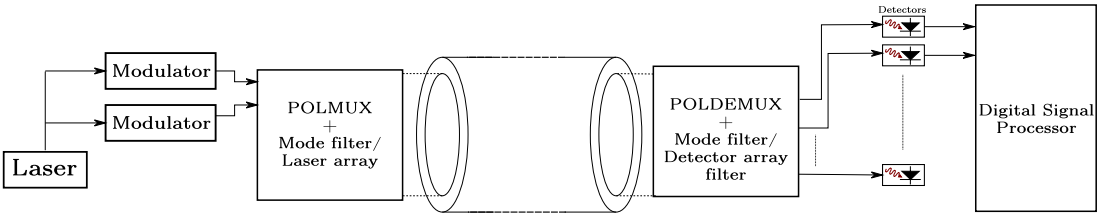

Fig. 1. Schematic depicting various components applicable for the model. The launch and detection portions are shown for a single laser and detector, respectively.

each of these corresponds to two launch and detect polarizations.

The modes of an optical fiber form a spanning set for the solutions of the Helmholtz wave equation. These eigenmodes of graded-index MMFs are the well-established Hermite–Gauss functions [37]. Thus, we can decompose an electric field distribution guided by the fiber into a linear combination of these eigenmodes with complex coefficients. While these modes are approximations for step-index MMFs, we restrict our consideration to graded-index MMFs that have lower dispersion. Using the basis of propagating modes, a vector that fully describes the electric field profile of a signal that propagates in the cross section of the fiber can be constructed. The entries of this vector are the projections of an incoming electric field profile at the input facet of the optical fiber onto each of the fiber eigenmodes. We refer to this as the "mode vector."

To find the mode vector for a particular laser/detector, we assumed that the device electric field is a circularly symmetric Gaussian beam (TEM_{00} mode) polarized randomly along the x-y plane (assuming that z is the propagation direction), and that the size of the beam reflects the effective area of the device. This assumption is motivated by the fact that small devices, such as vertical cavity surface emitting lasers (VCSELs), produce near-Gaussian beams and can be readily fabricated into two-dimensional (2D) arrays [38]. Let $E_L(x,y)$ be the incoming electric field due to a laser source polarized in the x-y plane, where the subscript L denotes a laser. The divergence of the laser beam is considered small, as the devices are assumed to be butt-coupled to the fiber face. Let $E_{(\tilde{p},\tilde{q})_F}(x,y)$ be the electric field distribution of the fiber eigenmode indexed by mode numbers $(\tilde{p},\tilde{q})$ and polarized in the x-y plane. Then the complex entries of the vector corresponding to the incoming electric field are given by [37]

$$a_{\tilde{p},\tilde{q}} = \frac{\langle E_L, E_{(\tilde{p},\tilde{q})_F}\rangle}{\sqrt{\langle E_L, E_L\rangle\langle E_{(\tilde{p},\tilde{q})_F}, E_{(\tilde{p},\tilde{q})_F}\rangle}},$$
$$\text{where } \langle A,B\rangle = \int_{\mathbb{R}}\int_{\mathbb{R}} A(x,y)B^*(x,y)\mathrm{d}x\mathrm{d}y. \tag{1}$$

Subsequently, we relabel the admissible mode pairs $(\tilde{p},\tilde{q})$ with $1,\ldots,M$, where M is the total number of spatial modes. Using the overlap integral, the input vector can be found as follows:

$$\underline{a}_L = \begin{bmatrix} \langle E_L, E_{F_1}\rangle \\ \langle E_L, E_{F_2}\rangle \\ \vdots \\ \langle E_L, E_{F_M}\rangle \end{bmatrix}, \tag{2}$$

where $\underline{a}_L$ is an $M\times 1$ vector of complex numbers, with M being the total number of spatial and polarization modes propagating in the fiber. The number of modes supported by an optical fiber depends on the core diameter, the wavelength of light, and the differences in refractive indices of the core and cladding [1]. The fiber was assumed to be a graded-index fiber, consistent with the model in [5], with a radial refractive index profile n given by

$$n^2 = n_{0(x,y)}^2 - 2\Delta n_0^2\left(\frac{r}{a}\right)^{\alpha}, \tag{3}$$

where n_0 is the nominal refractive index at the fiber center, r is the radial distance, a is the fiber radius, n_0x, n_0y are the refractive indices for the x and y polarizations that differ by the birefringence, and Δ is the index difference between the core and cladding. The radial refractive index power law profile is characterized by $\alpha\approx 2$. With this assumption, the number of modes increases with increasing core diameter. For instance, a weakly guided MMF with a diameter of 50 μm, nominal refractive index of 1.45, and core-cladding refractive index difference of 0.01 supports 55 guided spatial modes at 1550 nm. We restrict our consideration to linearly polarized (LP) Hermite–Gauss modes, since these modes effectively approximate propagation in weakly guiding MMFs under the infinite-core approximation [39]. The electric field is polarized in the cross section of the fiber and contains x and y components for each of the guided modes of the fiber. In other words, accounting for the two states of polarization of each spatial mode, the fiber possesses a

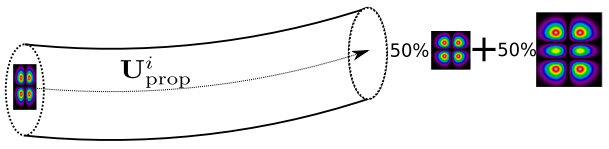

Fig. 2. $\mathbf{U}^i_{\text{prop}}$ is a random matrix that describes intermodal coupling within a section. In particular, it transforms a vector containing the weights of each guided mode to provide a vector that has the new weights after the signal has undergone intermodal coupling within the fiber section.

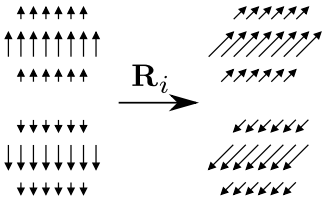

Fig. 3. $\mathbf{R}^i$ is a random matrix that describes rotation of the polarization of the electric field at section junctions. It rotates the polarization of each mode within the fiber section based upon propagation effects of the fiber.

total of $M = 55 \times 2 = 110$ modes. Thus, M defined here is the number of guided spatial and polarization modes in the fiber, and our model takes into account polarization variations of each mode. The simulations performed in this paper assumed a source wavelength of 1550 nm, since this wavelength lies in the lowest loss window of the fiber.

Once an input vector is determined, an $M \times M$ propagation matrix $\mathbf{U}_{\text{total}}$ transforms the input electric field vector into the output electric field vector. The propagation matrix includes information about the power transfer between the eigenmodes and losses incurred during propagation from fiber perturbations. Decomposing the fiber into N infinitesimally short, cascaded sections, a propagation matrix can be found for each of the i sections, $\mathbf{U}^i_{\text{section}}$. This matrix captures the impact of the energy transfer across the fiber modes, given by $\mathbf{U}^i_{\text{prop}}$ (Fig. 2); polarization rotation during propagation through the section, given by $\mathbf{R}^i$ (Fig. 3); and mode rotation due to fiber twists, given by $\mathbf{M}^i$ (Fig. 4). Multiplying these together yields the total propagation matrix $\mathbf{U}_{\text{total}} = \prod_{i=1}^{N} \mathbf{U}^i_{\text{section}}$, where $\mathbf{U}^i_{\text{section}} = \prod_{i=1}^{N} \mathbf{M}^i \mathbf{R}^i \mathbf{U}^i_{\text{prop}}$. The details of the assumptions and parameters of the simulation are discussed in Section V.

III. Analysis of MIMO System Matrix

In this section, we derive a MIMO system matrix model from the propagation framework for the MMF discussed in the previous section. Subsequently, we use this model to analyze how device placement can affect the performance of the link from a signal processing purview, and examine and design optimal laser and detector placement strategies to improve achievable data rates through the MMF.

A. System Transfer Matrix

To derive a MIMO channel matrix, for each laser and detector in the configuration, an input vector describing its

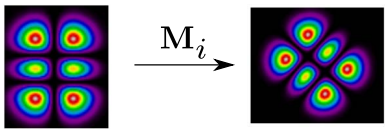

Fig. 4. $\mathbf{M}^i$ is a random matrix that describes rotation of the electric field profile due to fiber twists within the ith fiber section.

electric field profile can be formed using the techniques of Section II. These can be combined to obtain an effective channel matrix that describes the MIMO input–output channel state from the transmitter to the receiver. Performance metrics, such as information theoretic capacity and rate, can be calculated with this MIMO matrix. Such models can be used to evaluate the effectiveness of a particular laser/detector configuration in terms of information theoretic rate.

We assumed that the time-varying matrix $\mathbf{U}_{\text{total}}$, describing the modal transformation induced by the MMF, changes slowly with time. This enables estimation of the fiber transformation and compensation for its effects [7,21,40]. The implication of this assumption on the optimization metric considered is discussed in Section IV. The effects that these changes cause on the data rate are factored into our model.

Using the overlap integral technique described in Eq. (2), the input coupling vectors of each of the N_L lasers, represented as $\underline{a}_{L_1}, \underline{a}_{L_2}, \ldots, \underline{a}_{L_{N_L}}$, can be found. The output coupling vectors describing the overlap of different modes with each of the N_D detectors, represented by vectors $\underline{a}_{D_1}, \underline{a}_{D_2}, \ldots, \underline{a}_{D_{N_D}}$, can also be calculated similarly. To facilitate the evaluation of the MIMO intensity impulse response, we first find the principal modes of the system, referred to as $\underline{p}_i$, using the approach described in Subsection II.G of [5], and then evaluate the intensity impulse response using Eqs. (35) and (36) in the same reference, with a modification that the intensity impulse response is evaluated with the appropriate field pattern. In other words, to find the channel response between the ith laser and the jth detector, we compute

$$h_{ji,k}(t) = \sum_{k=0}^{2M} \langle \underline{a}_{D_j}, \underline{p}_k \rangle \langle \underline{p}_k, \underline{a}_{L_i} \rangle \delta(t - \tau_i), \tag{4}$$

where τ_i are the group delays of the respective principal modes. The group delays for each principal mode were calculated from the group delay operator operating on the $\mathbf{U}_{\text{total}}$ matrix, as described in Eq. (34) of [5]. The consolidated $h_{ji}(t)$ elements form the entries of the $\mathbf{H}(t)$ matrix, which provides the intensity impulse response of the MIMO system. The use of incoherent detection with conventional modulation results in cross-terms in the channel response, though the impact of these terms does not affect the data rate significantly for the length ranges concerned with intesity modulation, as has been suggested theoretically [8,19] and experimentally [21,26].

This framework allows the input–output relationship to be described in a compact fashion with input signals $x_1, x_2, \ldots, x_{N_L}$, outputs $y_1, y_2, \ldots, y_{N_D}$, and detector noise $n_1, n_2, \ldots, n_{N_D}$ as

$$\begin{bmatrix} y_1(t) \\ y_2(t) \\ \vdots \\ y_{N_D}(t) \end{bmatrix} = \mathbf{H}(t) \begin{bmatrix} x_1(t) \\ x_2(t) \\ \vdots \\ x_{N_L}(t) \end{bmatrix} + \begin{bmatrix} n_1(t) \\ n_2(t) \\ \vdots \\ n_{N_D}(t) \end{bmatrix}. \tag{5}$$

In the equations above, $x_i(t)$, $1 \le i \le N_L$, modulate the ith laser, while the signals $y_j(t)$, $1 \le j \le N_D$, are received at the jth photodetector. Although the lasers are modulated with the intensity modulation, we assume that the signals in the equation represent the baseband equivalent of the transmitted rf signal, as described in [41], thus permitting the use of complex modulation symbols. To analyze the performance of the MIMO system, we assumed that the system is in the thermal noise limited regime, as opposed to being shot noise limited. Therefore, the additive noise was modeled as white and Gaussian [26,41]. To factor in the effect of dispersion, the achievable rate was evaluated over various frequency bins, assuming that the channel remained flat within each bin, and these were integrated to get a net rate result, as shown in Fig. 5. The frequency bin for each flat subchannel was chosen to be 100 MHz, and rate values were evaluated up to 10 GHz, beyond which dispersion effects made the frequency response insignificant from a data rate perspective. We determined that using a frequency-domain bin size of 100 MHz provides a sufficiently accurate evaluation of the frequency-domain integral. In practice, such an implementation can be realized by using frequency-domain modulation techniques, such as orthogonal frequency division multiplexing [32].

In the following subsection, we briefly describe the metrics considered and the techniques adopted to optimize device geometries for increasing data rates.

B. Metrics for Optimization of Device Configurations

The primary metric of concern for optimizing the configurations of laser and detector arrays is the maximum achievable data rate through the fiber. For characterizing the potential data rate through the fiber, we considered the ergodic rate achievable over the fiber channel without channel state knowledge at the transmitter, given by [4]

$$C = \mathbb{E}\left[\log_2 \det\left(\mathbf{I}_{N_D} + \frac{\rho}{N_L}\mathbf{H}\mathbf{H}^H\right)\right] \text{ [b/s/Hz]}, \quad (6)$$

where $\mathbf{I}_{N_D}$ is the $N_D \times N_D$ identity matrix, ρ is the signal-to-noise ratio (SNR), and det represents the matrix determinant operation. This capacity formula can be used under our direct-detection-based channel model due to the fact that we operate the system in the thermal noise dominated regime, rather than the shot-noise limited regime, and the nonlinear interactions among the modes are negligible at the length scales considered in this paper [41]. Our analysis assumed a narrow frequency band signal within each subband. Thus, the rate could be obtained in bits-per-second by integrating it over the frequency response of the channel, as described in the previous subsection.

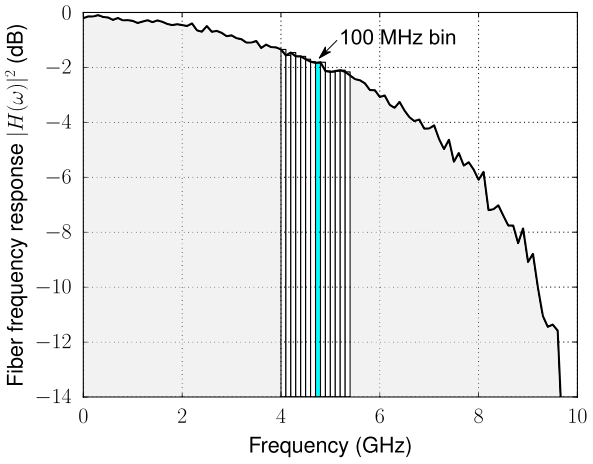

Fig. 5. Binning approach to evaluate the sum rate achievable over the fiber across all frequency ranges. The frequency response of the fiber channel was split into several bins of 100 MHz each, and the rate was evaluated within each bin assuming a frequency-flat channel response, and added up to get the net rate. This can be thought of as a frequency division multiplexing approach to rate evaluation.

Ergodic capacity is defined as the maximum rate that is obtainable through the fiber channel averaged over all realizations of the channel state $\mathbf{H}$, optimized over all input distributions. Therefore, it is based solely on the statistics of the channel, as opposed to specific realizations of channel states. In the case of a Gaussian MIMO channel whose channel matrix coefficients are i.i.d. Rayleigh entries, it has been shown that using i.i.d. Gaussian signaling on each transmit antenna is optimal [42]. However, for the MIMO-MMF channel considered in this chapter, the structure of the input–output relationship obtained by placing lasers and detectors in an array complicates the characterization of the input distribution that attains the ergodic capacity. In general, obtaining the optimal input distribution that achieves the ergodic capacity would require numerical computation of the input covariance. Thus, we restrict ourselves to using the achievable ergodic rate using Gaussian signaling with an identity covariance matrix as our optimization metric. In practice, while the fibers undergo significant mode coupling among degenrate modes (mode groups [40]), the coupling across mode groups is weak, and the mode-dependent losses are small. Thus, the achievable ergodic rate can be expected to be a close approximation to the ergodic capacity of the fiber [5]. The details of these aspects are discussed in Appendix B. Multiplexing capabilities of fibers that are limited by mode-dependent losses have been discussed in [43].

It must be noted that operating close to the rate as characterized by Eq. (6) would require amplitude modulation and coherent detection. Intensity modulation allows modulation of only half of the laser waveform swing, and no ability to use the laser phase. The model that we considered uses the intensity modulation by restricting the data signals to be positive and real. Since it is known that the capacity trends with increasing modulators and detectors for incoherent detection show an increasing trend, similar to the coherent case, at high SNR [4], the ergodic rate trends with various device configurations are also representative of rate trends in systems that employ direct detection. Heavy intermodal coupling will restrict MIMO benefits over longer fiber lengths, but over MMFs of up

to 3 km, the negative impact of intermodal coupling among various mode groups has been demonstrated to be small [10].

IV. Optimizing Placement of Devices

In this section, we discuss two different grid-based techniques for obtaining the optimal laser and detector configurations that maximize the ergodic rate achievable over the channel. The first, an exhaustive search over all possible device placements, yields the highest achievable rate for the grid; however, this method required significant computation time and became prohibitive for fine grids. The second method, a submodular optimization by "greedy" selection, reduced the number of computations required for evaluating the detector array for a preselected laser configuration. With greedy selection, the rate obtainable with the resulting configuration is only guaranteed to be within a constant factor of the maximal (ergodic) rate for the grid under consideration. While this may appear to be a limitation, it enabled the design of detector configurations for finer grids where an exhaustive search was computationally not tractable with standard computational resources. Even in coarse grids where an exhaustive search can be used, the greedy algorithm resulted in a configuration that attained a rate fairly close (more than 90%) to the maximal rate, with fewer computations. This also motivates the development of dense arrays of detectors from which a subset can be selected dynamically to enable reduced complexity signal processing. For our analysis and ease of implementation, we restricted ourselves to circular lasers and detectors that formed arrays. However, to improve fill factors and adapt to other geometric constraints, we suggest an alternate mechanism in Subsection V.E to suitably adapt the resulting array structures. The techniques presented here are applicable for designing device arrays with grids of arbitrary geometries, but in this section, we have restricted the discussion to square grids to allow for easy comparison between the various computational approaches.

A. Exhaustive Search

An exhaustive search for the optimal device configurations on an $N \times N$ square grid involves calculating the achievable rate of the channel for each possible combination of lasers and detectors on the grid positions and selecting the configurations that attain the highest rate. Letting the number of lasers be N_L and the number of detectors be N_D, this amounts to an exhaustive search over $\binom{N^2}{N_D} \times \binom{N^2}{N_L}$ possible device configurations. While this method always yields the maximum achievable rate for the channel, it requires significant computation for a fine grid or a large number of devices. For instance, using a 10×10 grid to determine the placement of 20 lasers and detectors would require $\binom{100}{20} \times \binom{100}{20} \approx 10^{41}$ comparisons. Thus, we restrict ourselves to applying exhaustive searches only on coarse grids.

B. Submodular Search

To design arrays with a larger number of devices, a finer grid structure of the fiber core region is necessary. However, as discussed in the previous section, determining optimal device placements was computationally prohibitive in such structures. We thus considered an alternative optimization technique, based on the observation that the rate function satisfies the property of "submodularity." Submodularity enables the use of a "greedy selection" algorithm that performs this optimization to within a constant factor of the global maximum, while requiring a significantly lower number of computations. In wireless MIMO systems, it is known that the problem of selecting a subset of antennas at the receiver for signal detection is submodular [28]. In the MMF case, the link rate is observed to be submodular with respect to the grid of detectors chosen, while keeping the laser configurations fixed. Let the set of potential detector locations on the $N \times N$ grid be indexed by the set $U = \{1, 2, \ldots, N^2\}$. The definitions and performance of submodular optimization are clarified in the theorems below.

Theorem 1. *The ergodic rate achievable over a MIMO link with no channel state information (information about the channel matrix* $\mathbf{H}$*) at the transmitter given in Eq. (6) is submodular in the choice of the subsets of receive devices (detectors) chosen. In other words, if the rate achievable at SNR* ρ *for a subset of receive devices* S *of size* N_D*, denoted by* R_S*, is given by*

$$R_S = \log_2 \det\left(\mathbf{I}_{N_D} + \frac{\rho}{N_D}\mathbf{H}_S\mathbf{H}_S^{\dagger}\right), \tag{7}$$

where $\mathbf{H}_S$ *is the submatrix obtained from the rows and columns with indices in* S*, and* $\mathbf{H}_S^{\dagger}$ *represents the Hermitian transpose of* $\mathbf{H}_S$*, then* R_S *is submodular in* $S \subseteq U$*. In addition, the function is monotone in the subsets; i.e., for* $S \subseteq T \subseteq U$*, if* R_T *is the rate achievable at SNR* ρ *with a subset of receive devices* T*, then we have* $R_T \geq R_S$*.*

The proof for this theorem is provided in Appendix A. The fact that the rate is submodular in the subset of detectors used leads to a performance guarantee with the use of Algorithm 1, which is based on greedy selection.

Algorithm 1: Greedy Selection Algorithm

initialize $S = \emptyset, U = 1, 2, \ldots, N^2$
for $i = 1$ to N_D **do**
  select $d = \underset{x \in U \setminus S}{\operatorname{argmax}}(R_{S \cup \{x\}} - R_S)$
  set $S = S \cup \{d\}$
end for
return S

Theorem 2. *Let* R^* *be the achievable rate when the* N_D *detectors are placed in the best of* N^2 *grid locations, and* R_S *be the data rate achievable with detectors placed at the*

locations given by the set S of size N_D, the output of the greedy selection approach described by Algorithm 1. Then we have

$$R^*(1-e^{-1}) \le R_S \le R^*. \tag{8}$$

The proof for the general case of Theorem 2 is provided in several texts, including [44].

Theorem 3. *The achievable ergodic rate of the multidevice link with no channel knowledge at the transmitter, which is*

$$\mathbb{E}[R_S] = \mathbb{E}\left[\log_2 \det\left(\mathbf{I}_{N_D} + \frac{\rho}{N_L}\mathbf{H}_S\mathbf{H}_S^{\dagger}\right)\right]$$

(*where the expectation is over the probability distribution of* $\mathbf{H}$), *is submodular and monotonic in the choice of the subsets of receive devices (detectors)* $S \subseteq U$.

Proof: Since Theorem 1 holds for each $\mathbf{H}$, and a linear combination of submodular functions is submodular, the ergodic rate is submodular. Since monotonicity is also proved pointwise, the ergodic rate is also monotone in the choice of the receive devices. ∎

It must be noted that the submodular optimization technique is useful only for optimizing detector configurations for a predetermined laser array configuration. This is because the submodularity of the MMF link rate does not extend to subsets of lasers selected from a grid. Thus, when utilizing submodular optimization, we restricted the analysis to predetermined laser configurations and focused on optimizing the detector configurations. The restriction of structure imposed due to submodularity did not allow laser positions to be optimized using this technique. Although this appears to be a limitation, significant performance benefits can be obtained even with regular geometries for laser arrays [45]. For finer grids, an exhaustive search was prohibitive, and submodularity provided an alternate and more viable solution. In fact, the rate obtained using a greedy search was guaranteed to be within a factor of $(1-e^{-1})$ of that obtained with the optimal detector array searched exhaustively. This provides a computationally feasible way to search for device configurations that are reasonably close to optimal for fine grids. Without additional structure in the problem, a performance guarantee better than $(1-e^{-1})$ cannot be obtained with a polynomial-time algorithm. It can be proven that with just submodularity and no additional structure, obtaining *any* guarantee on optimality better than a factor of $(1-e^{-1})$, i.e., a guarantee of $(1-e^{-1})+\epsilon$ for any $\epsilon > 0$, would require exponentially large computational resources for the most general optimization problems [46].

V. Simulation Results

We performed simulations on MATLAB to optimize laser and detector configurations that yielded the greatest ergodic rate over the ensemble of channel realizations under various scenarios. From Section III, for a given configuration, the system matrices $\mathbf{H}$ are derived from $\mathbf{U}_{\text{total}}$ matrices. An ensemble of randomly generated $\mathbf{U}_{\text{total}}$ matrices corresponds to the ensemble of system realizations and, thus, to an ensemble of system matrices $\mathbf{H}$. We generated 700 realizations of $\mathbf{U}_{\text{total}}$ matrices. To generate each $\mathbf{U}_{\text{total}}$, the model split the graded-index fiber into 10,000 sections, each 10 cm in length. The fiber had a diameter of 50 μm, a core refractive index of 1.444, and a numerical aperture of 0.19. The lasers were assumed to operate at a wavelength of 1.55 μm, and the spatial electric field pattern they produced was assumed to be circularly symmetric. The choice of 1550 nm was made since this wavelength band has a low propagation loss through the fiber. In addition, the field propagation approach for modeling MMF behavior has been experimentally shown to be accurate [2]. In each iteration of the simulation, a new realization of the fiber channel was used, wherein the transformation affected by the fiber was calculated anew to obtain a statistical average over several channel realizations. This was done to obtain meaningful estimates of the data rate supported by the fiber while modeling temporal variations affected by the fiber channel. Since the lasers were modulated incoherently, the phase with which each laser signal was launched was randomly chosen over each run of the simulation. The detectors' response was evaluated based on the overlap of the received signal on each detector. The statistical nature of the fiber is a result of the curvature and twists in each section, which are modeled by parameters κ_i and θ_i, respectively. Both are modeled as Gaussian random variables with κ_i having a standard deviation of 0.95 m^{-1} and θ_i having a standard deviation of 0.6 radians. These parameters were determined by correlating experimentally observed beam profiles obtained after propagation through a 1 km graded-index MMF for tuning the model to match physical parameters. An example of simulated and physical realizations of the fiber beams is provided in Fig. 6. The 10 cm fiber sections that the model considers are sufficiently small in comparison to the radius of curvature of the fiber, thus being effective in characterizing modal propagation effects [5]. For the parameters of the fiber, the differential group delays of the fiber modes ranged from 0 to 12 ns, consistent with measured channel parameters for such fibers [47]. To simplify the simulation complexity in this study, the device configurations were restricted to 2D rectangular

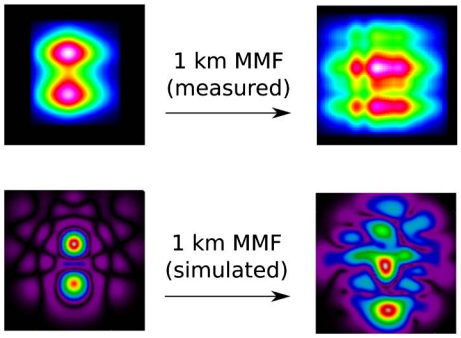

Fig. 6. Beam evolution over 1 km of graded-index MMF. The physical fiber measurement is performed using a beam profiler, while the simulated profile uses one channel realization obtained using the fiber model.

arrays centered about the fiber axis. The motivation for this assumption comes from the fact that the fabrication of devices with this geometry has been demonstrated in practice [38,48].

This section demonstrates two ways of enhancing the rate achievable over the channel. The first approach involves increasing the total number of lasers and detectors, and the second approach involves fixing the laser and detector positions of an $N_L \times N_D$ MIMO system selectively on the grid and showing the existence of an optimal device configuration on the grid. This optimal device configuration was found through exhaustive search over all possible device positions on the grid. For finer grids, an exhaustive search became computationally expensive. Instead, a suboptimal "greedy" search was performed for detector arrays, for a fixed laser array. We compared the values of the ergodic rates obtained using the exhaustive search and greedy search based algorithms for a coarse grid to establish its utility. Finally, the performance of the system in terms of an outage rate was also evaluated, to establish the utility of the configurations obtained by these methods in terms of outage.

A. Rate Benefits due to MIMO

To demonstrate the effect of increasing the number of devices on the rate achievable over the MMF link, simple segmented lasers and detectors were considered, as shown in Fig. 7. The mode-field diameter of the lasers and detectors

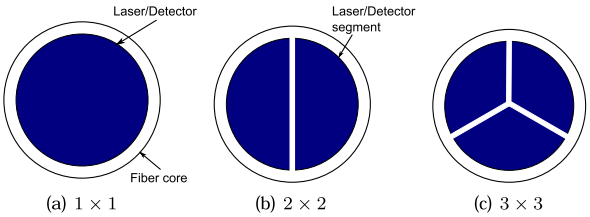

Fig. 7. Multiple lasers and detectors. The devices were assumed to fill 90% of the fiber core area.

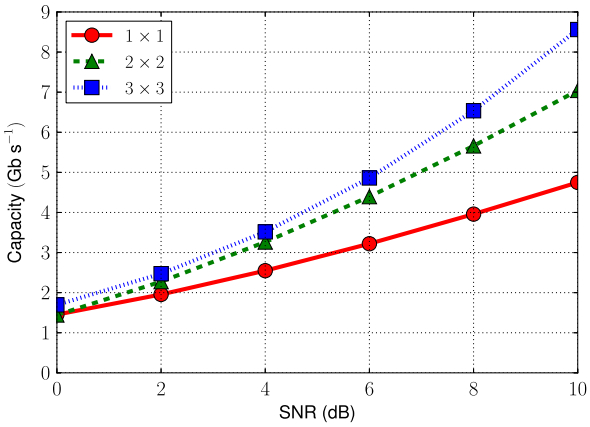

Fig. 8. Achievable rate versus SNR for 1×1, 2×2, and 3×3 MIMO systems for the best device configuration.

was assumed to be 45 μm, and the ergodic rate was evaluated for 1×1, 2×2, and 3×3 links with these laser and detector geometries. In each case, the achievable rate was averaged over 700 randomly generated system matrices that represented the channel conditions to obtain the ergodic rate, as stated in Eq. (6). The results of this simulation are shown in Fig. 8. Such simple segmented lasers and detectors may not necessarily be the optimal geometries to extract the maximum data rate from the MIMO link; nevertheless, the results of this simulation indicate that a significant increase in data rates can be obtained with MIMO techniques. Compared with a 1×1 system at 10 dB SNR, the optimal 2×2 and 3×3 implementations yielded gains of 40% and 80%, respectively, supporting the claim that when an increasing number of devices is used, the rate improves significantly.

In the system descriptions below, each transmit and receive stream utilizes the polarization degree of freedom, as shown in Fig. 1. So, when we refer to an $N_T \times N_R$ system, the implementation would effectively consist of $2N_T$ transmit streams and $2N_R$ receive streams. For simplicity, we omit the factor of 2 in the subsequent discussions.

B. Effect of Device Positions on Capacity Using Exhaustive Search

To examine how the achievable rate over a $N_L \times N_D$ MIMO system can be increased with appropriate choice of laser and detector positions, a 3×3 grid was used as an example for optimizing the geometries of 2×2 and 3×3 MIMO systems. The average rate was found for each combination of two (or three) lasers and two (or three) detectors on the grid. Since the actual overlap integral determines the power received by the detectors, the joint optimization provides the best simultaneous laser and detector configuration that optimizes the power coupling into the modes of the fiber and provides the best receiver sensitivity, while obtaining the highest data rate using multiplexing. From a practical standpoint, the performance under such coupling constraints would be comparable to free-space coupling based approaches in few-mode fiber and MMF [11,34], although the large core of the MMF facilitates better offset tolerances [49]. Figure 9(a) shows the rate versus SNR of a 2×2 MIMO system for the best combination, and compares it with the average rate over all possible positions of lasers and detectors. The rate obtained using the best arrangement of devices far exceeds that obtained when the device placement is done randomly, as is clear from the fact that the rate averaged over all positions is significantly smaller. In this case, the data rate of the best configuration at an SNR of 10 dB is more than twice that of the average over all configurations. The location of the lasers and detectors that obtains the best rate is shown in Fig. 9(b). A similar analysis was performed for a 3×3 MIMO system with the results shown in Fig. 10(a). From the figure, it can be seen that if the best configuration is chosen at an SNR of 10 dB, the data rate can be increased to more than twice the data rate obtained by averaging over all configurations for the 3×3 case. These simulation

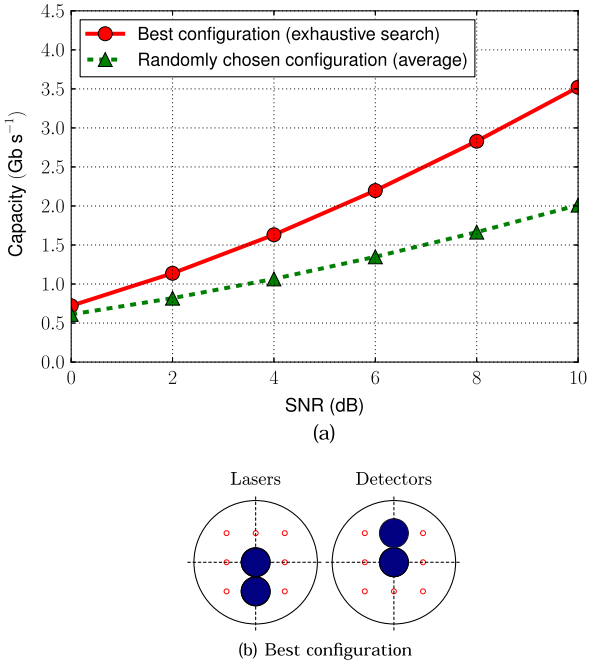

Fig. 9. (a) Achievable rate versus SNR for a 2×2 MIMO system for the "best" device configuration that achieves the highest rate and the average over all possible configurations. (b) Configuration of lasers and detectors in the best configuration. The four circles at the bottom represent the fiber cross sections and the laser and detector placements on the cross sections that yielded both the best and the suboptimal configurations.

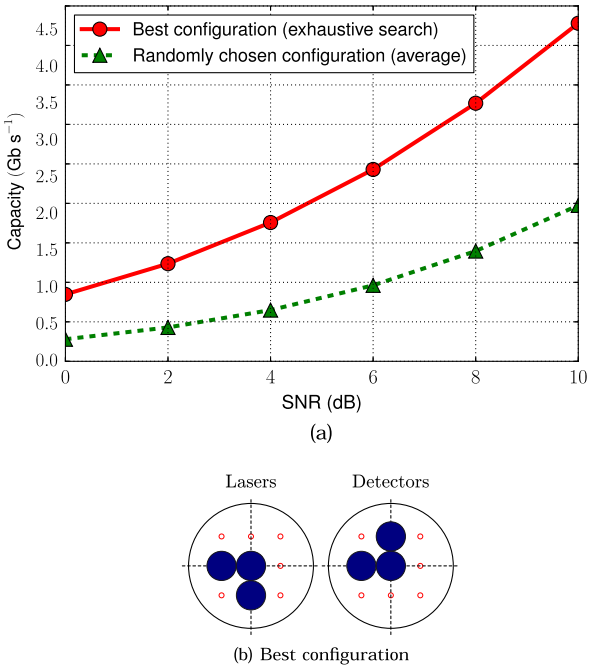

Fig. 10. (a) Achievable rate versus SNR for a 3×3 MIMO system for the "best" device configuration that achieves the highest rate and the average over all possible configurations. (b) Configuration of lasers and detectors in the best configuration.

results indicate that the maximum achievable data rate can be significantly increased with appropriately chosen configurations of laser and detector arrays. As most configurations of laser and detector positions on the grid result in suboptimal performance, it is essential to use a suitable configuration of device geometries to ensure good MIMO performance. The use of the polarization degrees of freedom roughly doubled the achievable rate, since polarization mode dispersion was negligible in comparison to modal dispersion at the fiber lengths considered in these models.

C. Comparison of Exhaustive and Greedy Search: Coarse Grids

As mentioned in Subsection IV.B, a "greedy" selection can be used to find the best configuration of detectors in finer grids, where an exhaustive search is computationally expensive. To demonstrate the usefulness of the search technique and to provide an example of the data rates that result from it, an illustrative case with small numbers, a 5×5 MIMO system used on a 5×5 grid, was evaluated. For such a system, an exhaustive search is computationally reasonable. However, even for this small grid and MIMO system, an exhaustive search requires $\binom{25}{5} = 53{,}130$ comparison operations, while a greedy search requires only ~115 comparisons. The positions of the five lasers were chosen as in Fig. 11(a). Given this placement of lasers, an exhaustive search selected a detector configuration

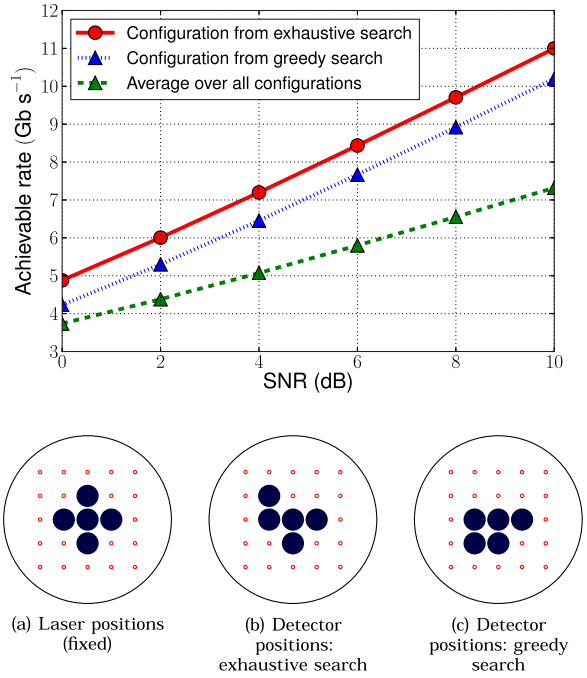

Fig. 11. Comparing the configurations obtained by the exhaustive search and the greedy search. It can be observed that about 92% of the rate of the optimal exhaustive search can be obtained by the greedy search in this case.

shown in Fig. 11(b), and a submodular search selected a detector configuration as shown in Fig. 11(c). From the plot in Fig. 11, at an SNR of 10 dB, the rate of the channel using the greedy configuration yielded roughly 92% of the optimal rate obtained by an exhaustive search, while requiring only ∼0.2% of the comparisons. For reference, the average of the rate over all positions is also presented, and it is significantly lower than the rate achievable with the configurations obtained by the exhaustive and greedy selection procedures. As the grids are made finer, with a larger number of potential locations to place detectors, a greedy search requires a significantly lower number of comparisons while guaranteeing at least a $(1-e^{-1})$ factor of the rate obtained with the optimal configuration, making the submodular technique useful in such situations. While this discussion focuses on developing efficient static arrays of detectors using the greedy selection technique, one could also employ this technique on a dense grid of detectors to dynamically select a subset of detectors for reduced complexity MIMO signal processing while retaining all the diversity benefits of a fine-grained array of detectors.

The analysis above was conducted using the achievable ergodic rate as the metric. However, modern optical fiber links that use multiplexing and support high availability demands are likely to be limited by outage [34,36,43,50,51]. Thus, we compare the laser/detector configurations and rate performance obtained with outage as the metric.

Using an approach similar to the one described above, the achievable rate at an outage probability p_{out} of 10^{-2} was used as the metric to obtain the optimal laser/detector configurations. To evaluate the outage rate, several channel realizations $\mathbf{H}$ were generated for a given $N_L \times N_D$ configuration, and for these realizations, the largest achievable rate R satisfying

$$p_{\text{out}} = \mathbb{P}\left[\log_2 \det\left(\mathbf{I}_{N_D} + \frac{\rho}{N_L}\mathbf{H}\mathbf{H}^H\right) < R\right] \tag{9}$$

was evaluated. For the SNRs considered in these simulations, it was observed that the best configuration in terms of outage matched the configuration obtained using ergodic rate as the metric, as shown in Fig. 12. This

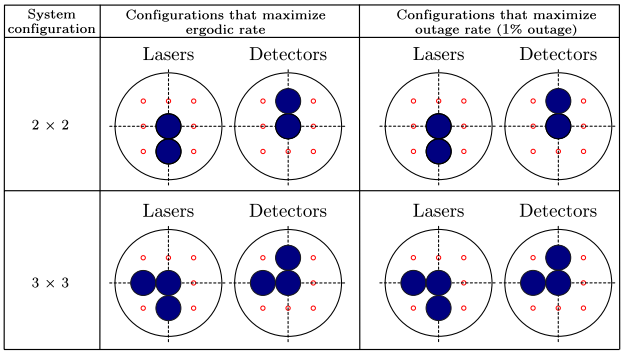

Fig. 12. Similar configurations are observed with both the outage rate and the ergodic rate as metrics for optimizating the laser/detector configurations.

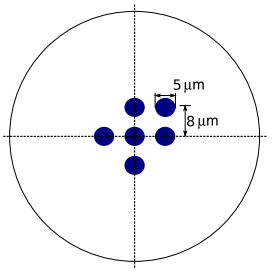

Fig. 13. Laser array utilized with the 50 μm fiber. The lasers have a mode-field diameter of 5 μm and a pitch of 8 μm.

can be attributed to the fact that the gap between outage and ergodic capacities generally diminishes at higher SNRs [52].

D. Detector Arrays Using Fine Grids and Greedy Search

Performing an exhaustive search to optimize detector geometries for a 6 × 6 MIMO system becomes computationally prohibitive with finer grids, such as a 7 × 7, 9 × 9, or 11 × 11 grids. For example, $\binom{49}{6} \approx 10^7$, $\binom{81}{6} \approx 10^8$, and $\binom{121}{6} \approx 10^9$ comparison operations are required for the 7 × 7, 9 × 9, and 11 × 11 grids respectively; in other words, the complexity of this task is $O(N^{N_D})$ in the Big-O notation [53], where N is the grid size and N_D is the number of detectors, making an exhaustive search a computationally expensive proposition. Therefore, we resorted to fixing a laser configuration and performing a submodular search on the detector configurations, which reduced the number of computations significantly. For instance, for placing six detectors in the 11 × 11 grid, only ∼711 comparisons are needed, which represents massive computation savings when compared to the optimal search requiring 10^9 comparisons. In other words, the greedy approach imposes a complexity of only $O(NN_D)$. As an example, we considered the placement of detectors for a 6 × 6 MIMO system with a fixed laser array as shown in Fig. 13.

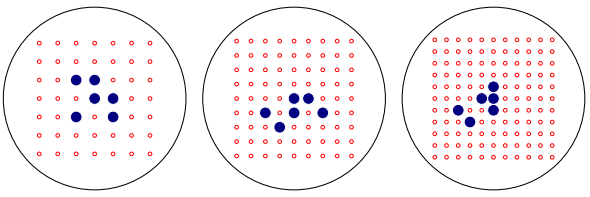

Fig. 14. Detector configurations obtained by the greedy algorithm for detectors of diameter 4 μm for various grid structures. Interestingly, there is a significant preference toward detectors closer to the fiber core, indicating the fact that much of the received power in graded-index MMFs propagates close to the axis.

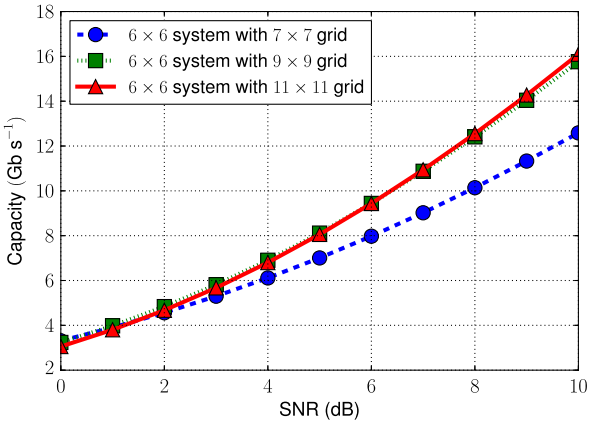

Fig. 15. Capacity trends obtained with the detector configurations shown in Fig. 14.

With this fixed laser configuration, we evaluated the rate obtainable over the link with six photodetectors, with each photodetector having a mode-field diameter of 4 μm, and obtained the best configuration by submodular optimization. The resulting detector array configurations obtained by simulation with these grid configurations are shown in Fig. 14. The data rate achieved by each of these configurations is shown in Fig. 15. It can be observed that the achievable rate improves for the 9 × 9 grid when compared to the 7 × 7 grid, due to the improved flexibility in placement of devices. However, the further improvement is marginal for the 11 × 11 case, indicating a trend of diminishing returns with increasing granularity of the grid structure. This trend can be attributed to the fact that the rate is dependent on choosing detector placements that overlap with high-intensity points at the output facet of the fiber. A 4 μm mode-field diameter for the detectors, chosen in accordance with the pitch of the grid structure, provides structures that cover the high-intensity points sufficiently for a 9 × 9 grid, and the finer detector positions offered by a 11 × 11 grid do not significantly improve the overlap, thus indicating diminishing returns with finer grid structures. So, while the use of finer grids for obtaining detector configurations is made possible using this approach, the diminishing returns obtained as the grids become finer indicate that extreme granularity of the grid structure is not necessary for obtaining good detector structures that provide MIMO benefits.

E. From Device Arrays to Segmented Detectors

While the simple device array models presented above confirm the utility of choosing an appropriate geometry for laser and detector arrays for MIMO-MMF systems, it is often desirable to employ detectors that possess a larger profile in order to improve the fill factor, and thereby increase the received SNR and reduce their susceptibility to speckle noise [19]. To this end, we used the fine grid simulation result as a template to build a consolidated laser/detector array that provided a much more robust solution

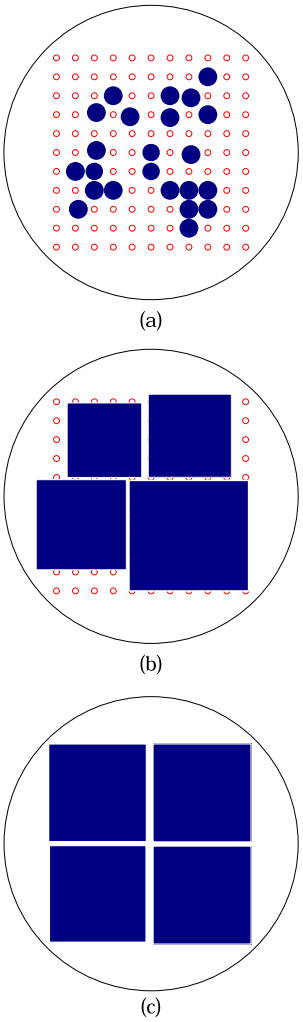

Fig. 16. (a) A fiber was analyzed to obtain the best 23 locations to place small circular detectors on a 11 × 11 grid as discussed in Subsection V.C. (b) Clustering these detectors to obtain larger square segments to improve the fill factor. (c) Regular four-element detector array without using the design from the algorithm.

to capturing a large fraction of the received signal. We describe this technique using an example.

Figure 16(a) shows the result of the algorithm described in Subsection V.C for a 11 × 11 grid, with the circles indicating ideal locations for 23 detectors. The algorithm obtained a detector array that possessed a poor fill factor of about 1%. While the diversity benefit offered by 23 detectors is high, the SNR required to reap these benefits is also prohibitively large. This can be attributed to the fact that the higher-order modes of the MMF have mode structures that do not permit easy coupling without the use of densely clustered systems for launch and detection. Although the use of spatial light modulators and dense detector arrays can permit effective access to higher-order modes of the fiber, the ability to detect a sufficient amount of power at the receiver's small detectors is severely restricted. To overcome this fundamental limitation imposed by the spatial geometry of the modes of

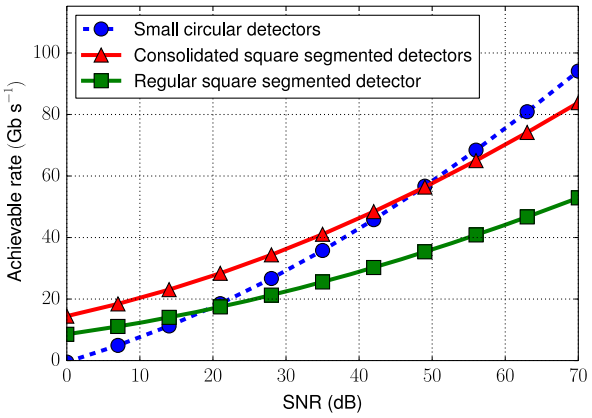

Fig. 17. Comparison of capacity trends for the detector patterns shown in Fig. 16.

large-core MMFs, we suggest an alternate strategy for effectively consolidated detector structures that can provide diversity gains while detecting enough power at the receiver.

Based on our observation from the simulated and experimentally observed fiber characteristics, we assumed that neighboring detectors receive fairly correlated signals, and by combining these detectors that receive correlated signals into one block, the diversity benefit is not significantly diminished, but the SNR is greatly improved. In the current example, we clustered the detector locations in Fig. 16(a) into four sectors, and obtained a new configuration shown in Fig. 16(b), significantly improving the fill factor. We restricted the choice to square segments for implementation ease.

The predicted performance of these systems is shown in Fig. 17, where we considered a system with one laser at the transmitter and various configurations at the receiver; here, Fig. 16(a) shows the detector configuration for the "small circular detectors" array, Fig. 16(b) represents the detector system shown as "consolidated square segmented detectors," and, finally, Fig. 16(c) shows a "regular square segmented detector" array constructed without the optimization procedure. We observed that the fill factor improvement is significant for both of the square array structures, where the rate is about 3.5× the rate achievable with the small circular detector array at an SNR of 0 dB. However, the slope in the rate curve is diminished, and at very high SNRs (in excess of 50 dB), the performance of the square arrays falls due to the loss in diversity. Despite this limitation, over a practical range of SNRs, the consolidated detector array significantly outperforms both the small circular detectors and the regular detector system, which does not possess as much of a diversity advantage as the circular and consolidated square arrays.

While the device geometry design algorithm presented in Subsection III.B generates array structures that are efficient from a diversity perspective, the small fill factors of resulting arrays could make them unsuitable for practical use owing to their susceptibility to speckle noise. By effectively consolidating the structures obtained from the algorithm, useful detector arrays that possess a high fill factor, while still providing diversity benefits over regular detector structures, could be obtained. Such lasers and detector geometries, whose laser/detector diameters are about 10–15 μm, match closely with commercially available components, and can be used to enhance multiplexing through large-core MMFs using offset coupling with SMFs [24,54]. While a lens-based system can be used to couple an array of photodetectors that is larger in size, such as the arrays described in [55], this could make the system unwieldy and difficult to realize. Better approaches to avoiding the problem of dense arrays of detectors exist, using alternate strategies to couple from the fiber into photodetectors. One such approach could involve the use of spot-based couplers that have been demonstrated to be useful in few-mode fiber based systems [56]. Photonic lanterns [57] and MMF ribbon structures [58] could also be used as effective mode filters at the receiver to couple to large detector arrays without increasing the system complexity significantly [59]. Such approaches permit the use of large, dense arrays of photodetectors, without imposing tighter alignment tolerances. With developments in device technology, 2D arrays of devices that satisfy geometric constraints have already been fabricated in [38,48]. Further developments in fabrication technology are likely to yield device arrays that can further access the diversity benefits provided by the fiber, and enhance the achievable data rates through large-core MMF links.

VI. Conclusion

We have developed a statistical channel model for a MIMO-based MMF link that is capable of quantifying the impact of the geometry of laser and detector arrays on the achievable data rate. Such an input–output signal processing model enables us to analyze the achievable rate over a MMF link containing multiple lasers and detectors. In particular, we provided a means to analyze the link performance with particular geometries of laser and detector arrays, and emphasized the importance in designing appropriate arrays of devices for maximum performance. With ergodic rate as the design criteria, we numerically determined the optimal device arrays for coarse grids under appropriate feasibility constraints using an exhaustive search. These simulations revealed that systems with optimal device configurations could outperform arbitrarily chosen device arrays by more than 200%. For finer grids, an optimal exhaustive search becomes computationally demanding due to a large number of comparisons. On the other hand, a submodular "greedy" algorithm, which is guaranteed to yield a rate within a factor $(1-e^{-1})$ of the rate achievable with the optimal configuration, is used to alleviate complexity. Optimal exhaustive searches for device geometries were compared to greedy searches, and this revealed that device configurations that attain more than 90% of the rate achievable with optimal exhaustive search could be obtained with less than 0.2% of the comparisons for fine grids, illustrating the potential utility of the greedy search. The high performance and low

complexity of the greedy search make it an effective tool for implementing dynamically reconfigurable detector arrays with reduced digital signal processing (DSP) complexity. To address the issue of low fill factors with the detector structures obtained from the algorithm, we provided a method to consolidate several detectors to obtain segmented detectors with improved fill factors while retaining diversity benefits. Future work will involve experimental verification of these concepts as well as an extension to other guided media, such as plastic fibers.

Appendix A: Proof of Theorem 1

To allow the results presented in this paper to be self-sufficient, we provide the proof for the submodularity results used in this paper. The MIMO information theory related notation closely follows the notation used in [4].

Theorem 4. *The entropy of a random vector* $\mathbf{X} = [X_1, X_2, \ldots, X_n]$ *is submodular in the choice of subsets of* $\{X_1, X_2, \ldots, X_n\}$.

Proof: Let h denote the entropy of a random vector. We note that a sufficient condition for the entropy to be submodular in the subsets of the elements of $\mathbf{X}$ is

$$h(\mathbf{X}_{A\cup B}) + h(\mathbf{X}_{A\cap B}) \geq h(\mathbf{X}_A) + h(\mathbf{X}_B) \quad \forall\, A, B \subseteq \{X_1, X_2, \ldots, X_n\}.$$

We prove this below.

To denote subsets of the random vector, we use the notation $\mathbf{X}_A = \{X_i : i \in A\}$, where $A \subseteq \{1, 2, \ldots, n\}$. Let A and B be subsets of $\{1, 2, \ldots, n\}$. With this, we have

$$\begin{aligned} &h(\mathbf{X}_{A\cup B}) + h(\mathbf{X}_{A\cap B}) - h(\mathbf{X}_A) - h(\mathbf{X}_B) \\ &\quad = [h(\mathbf{X}_A) + h(\mathbf{X}_{B\setminus A}|\mathbf{X}_A)] + h(\mathbf{X}_{A\cap B}) - h(\mathbf{X}_A) - h(\mathbf{X}_B) \\ &\quad = h(\mathbf{X}_{B\setminus A}|\mathbf{X}_A) + h(\mathbf{X}_{A\cap B}) - [h(\mathbf{X}_{A\cap B}) - h(\mathbf{X}_{B\setminus A}|\mathbf{X}_{A\cap B})] \\ &\quad = h(\mathbf{X}_{B\setminus A}|\mathbf{X}_A) - h(\mathbf{X}_{B\setminus A}|\mathbf{X}_{A\cap B}) \geq 0. \end{aligned}$$

Thus, this function is submodular. ∎

Proof of Theorem 1

Proof: We prove this by using Theorem 4 and making an observation on augmented matrices. Let ρ be the SNR of the received signal and N_D be the number of detectors. First, consider an $N_D \times 1$ complex Gaussian random vector $\mathbf{Z}$ whose covariance matrix is $\mathbf{R}_\mathbf{Z} = \mathbf{I}_{N_D} + (\rho/N_D)\mathbf{H}\mathbf{H}^\dagger$. We denote the subvector of $\mathbf{Z}$ consisting of the elements in the set S by $\mathbf{Z}_S$. Then entropy of this random vector is given by

$$\begin{aligned} h(\mathbf{Z}_S) &= \log((\pi e)^{|S|} \det(\mathbf{R}_{\mathbf{Z}_S})) \\ &= \log\left((\pi e)^{|S|} \det\left(\mathbf{I}_{|S|} + \frac{\rho}{N_D}\mathbf{H}_S\mathbf{H}_S^\dagger\right)\right) \\ &= |S|\log(\pi e) + C_S. \end{aligned}$$

Thus, for any set of receive devices S, we have

$$C_S = h(\mathbf{Z}_S) - |S|\log(\pi e).$$

We also note that the addition of a receive device (detector) to the system would transform the system matrix as follows, assuming the row x of $\mathbf{H}$, represented by $\mathbf{h}_x$, is added:

$$\mathbf{H}_{S\cup\{x\}} = \begin{bmatrix} H_S \\ \mathbf{h}_x \end{bmatrix},$$

which results in the new rate

$$\begin{aligned} C_{S\cup\{x\}} &= \log\ \det\left(\mathbf{I}_{|S|+1} + \frac{\rho}{N_D}\begin{bmatrix} H_S \\ \mathbf{h}_x \end{bmatrix}\begin{bmatrix} H_S^\dagger & \mathbf{h}_x^\dagger \end{bmatrix}\right) \\ &= \log\ \det(\mathbf{R}_{\mathbf{Z}_{S\cup\{x\}}}) = h(\mathbf{Z}_{S\cup\{x\}}) - (|S|+1)\log(\pi e), \end{aligned}$$

where $\mathbf{R}_{\mathbf{Z}_{S\cup\{x\}}}$ is the covariance matrix, a subvector of the random vector $\mathbf{Z}$ consisting of elements with indices given in $S \cup \{x\}$.

Consider now a set of receive devices T, such that $S \subseteq T \subseteq \{1, 2, \ldots, N_D\}$. We have

$$\begin{aligned} &C_S - C_{S\cup\{x\}} - (C_T - C_{T\cup\{x\}}) \\ &= h(\mathbf{Z}_{S\cup\{x\}}) - (|S|)\log(\pi e) - (h(\mathbf{Z}_S) - |S|\log(\pi e)) \\ &\quad - h(\mathbf{Z}_{T\cup\{x\}}) + (|T|)\log(\pi e) + (h(\mathbf{Z}_T) - |T|\log(\pi e)) \\ &= [h(\mathbf{Z}_{S\cup\{x\}}) - h(\mathbf{Z}_S) - (h(\mathbf{Z}_{T\cup\{x\}}) - h(\mathbf{Z}_T))] \\ &\geq 0 \text{ (due to the submodularity of entropy).} \end{aligned}$$

The last step follows from Theorem 4.

To prove monotonicity, we repeatedly utilize the fact that $\det(\mathbf{I} + \mathbf{AB}) = \det(\mathbf{I} + \mathbf{BA})$. We begin with

$$C_{S\cup\{x\}} = \log\ \det\left(\mathbf{I}_{|S|+1} + \frac{\rho}{N_D}\begin{bmatrix} H_S \\ \mathbf{h}_x \end{bmatrix}\begin{bmatrix} H_S^\dagger & \mathbf{h}_x^\dagger \end{bmatrix}\right).$$

Proceeding thus, we have

$$\begin{aligned} C_{S\cup\{x\}} &= \log\ \det\left(\mathbf{I}_{|S|+1} + \frac{\rho}{N_D}\begin{bmatrix} H_S \\ \mathbf{h}_x \end{bmatrix}\begin{bmatrix} H_S \\ \mathbf{h}_x \end{bmatrix}^\dagger\right) \\ &= \log\ \det\left(\mathbf{I}_{N_D} + \frac{\rho}{N_D}\begin{bmatrix} H_S \\ \mathbf{h}_x \end{bmatrix}^\dagger\begin{bmatrix} H_S \\ \mathbf{h}_x \end{bmatrix}\right) \\ &= \log\ \det\left(\mathbf{I}_{N_D} + \frac{\rho}{N_D}[H_S^\dagger H_S + \mathbf{h}_x^\dagger\mathbf{h}_x]\right) \\ &= \log\ \det\left(\mathbf{I}_{N_D} + \frac{\rho}{N_D}H_S^\dagger H_S\right) \\ &\quad + \log\ \det\left(\mathbf{I}_{N_D} + \left(\mathbf{I}_{N_D} + \frac{\rho}{N_D}H_S^\dagger H_S\right)^{-1}\mathbf{h}_x^\dagger\mathbf{h}_x\right) \\ &= \log\ \det\left(\mathbf{I}_{N_D} + \frac{\rho}{N_D}H_S^\dagger H_S\right) \\ &\quad + \log\left(1 + \mathbf{h}_x\left(\mathbf{I}_{N_D} + \frac{\rho}{N_D}H_S^\dagger H_S\right)^{-1}\mathbf{h}_x^\dagger\right) \\ &= C_S + \log(1+b), \quad \text{where } b \\ &= \mathbf{h}_x\left(\mathbf{I}_{N_D} + \frac{\rho}{N_D}H_S^\dagger H_S\right)^{-1}\mathbf{h}_x^\dagger. \end{aligned}$$

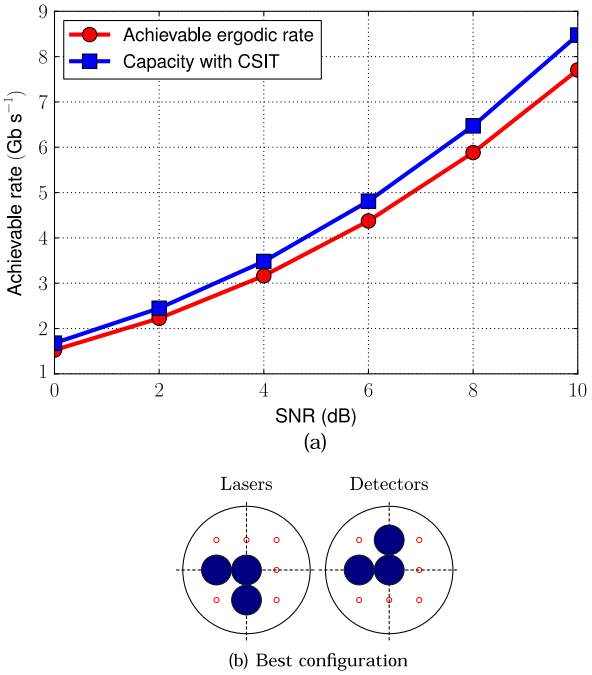

Fig. 18. (a) Capacity versus SNR for a 3 × 3 MIMO system for the "best" device configuration that achieves the highest rate and the average over all possible configurations. (b) Configuration of lasers and detectors in the best configuration.

Now, by observing that b is of the form $\mathbf{h}_x\mathbf{M}\mathbf{h}_x^\dagger$, where $\mathbf{M}$ is a positive semidefinite matrix, we have that $b \geq 0$, and thus $\log(1+b) \geq 0$. Thus, we may conclude that

$$C_{S\cup\{x\}} = C_S + \log(1+b) \geq C_S,$$

thereby establishing monotonicity. ∎

Appendix B: Gap Between Achievable Rate and Capacity

As discussed in Subsection III.B, to evaluate the information theoretic capacity of the fiber link with laser/detector arrays would require optimization over the distribution of the input covariance distribution. To compute the optimal input distribution that optimizes the rate requires a search over the set of all $N_T \times N_T$ covariance matrices that satisfy the power constraint. Since an evaluation of such matrices for each configuration is computationally expensive, we restricted ourselves to using the achievable rate with an identity covariance matrix. To verify this, we compared the achievable rate obtained with the laser/detector arrays with the capacity obtained with full channel state information at the transmitter (CSIT), since that is an overestimate of the ergodic capacity of the system with the optimal input distribution. An example is presented in Fig. 18 with two significant observations. First, the capacity with full CSIT and the achievable rate without CSIT follow a similar trend, and the achievable rate is not more than 10% below the capacity with CSIT. More significantly, the best configurations obtained using both metrics were configurations that were nearly identical in geometry (barring minor variations in laser/detector positions). Indeed, this was verified to be true for all configurations considered in this paper. Thus, we conclude that evaluating the achievable rate with a Gaussian input distribution with i.i.d. signaling on each of the N_T transmitters (identity covariance matrix) at the input is an appropriate metric for obtaining the best laser/detector arrays.

Acknowledgments

This work was presented in part at the IEEE International Conference on Communications, 2012, Ottawa, Canada. This work was supported by the National Science Foundation under an EAGER grant (EECS-1230034).

References

[1] G. Agrawal, *Fiber-Optic Communication Systems*, vol. 3. New York: Wiley, 1997.

[2] X. Shen, J. Kahn, and M. Horowitz, "Compensation for multimode fiber dispersion by adaptive optics," *Opt. Lett.*, vol. 30, no. 22, pp. 2985–2987, 2005.

[3] J. Peeters Weem, P. Kirkpatrick, and J. Verdiell, "Electronic dispersion compensation for 10 gigabit communication links over FDDI legacy multimode fiber," in *Optical Fiber Communication Conf.*, Anaheim, CA, 2005, paper OFO4.

[4] D. Tse and P. Viswanath, *Fundamentals of Wireless Communication*. Cambridge University, 2005.

[5] M. Shemirani, W. Mao, R. Panicker, and J. Kahn, "Principal modes in graded-index multimode fiber in presence of spatial and polarization-mode coupling," *J. Lightwave Technol.*, vol. 27, no. 10, pp. 1248–1261, 2009.

[6] H. R. Stuart, "Dispersive multiplexing in multimode optical fiber," *Science*, vol. 289, no. 5477, pp. 281–283, 2000.

[7] A. R. Shah, R. C. J. Hsu, A. Tarighat, A. H. Sayed, and B. Jalali, "Coherent optical MIMO (COMIMO)," *J. Lightwave Technol.*, vol. 23, no. 8, pp. 2410–2419, 2005.

[8] N. Bikhazi, M. Jensen, and A. Anderson, "MIMO signaling over the MMF optical broadcast channel with square-law detection," *IEEE Trans. Commun.*, vol. 57, no. 3, pp. 614–617, 2009.

[9] J. Siuzdak, "RF carrier frequency selection for incoherent MIMO transmission over MM fibers," *J. Lightwave Technol.*, vol. 27, no. 22, pp. 4960–4963, 2009.

[10] C. Tsekrekos, A. Martinez, F. Huijskens, and A. Koonen, "Mode group diversity multiplexing transceiver design for graded-index multimode fibres," in *31st European Conf. on Optical Communication (ECOC)*, vol. 3, Sept. 2005, pp. 727–728.

[11] R. Ryf, S. Randel, A. Gnauck, C. Bolle, R. Essiambre, P. Winzer, D. Peckham, A. McCurdy, and R. Lingle, "Space-division multiplexing over 10 km of three-mode fiber using coherent 6 × 6 MIMO processing," in *Optical Fiber Communication Conf.*, Los Angeles, CA, 2011, paper PDPB0.

[12] B. Zhu, T. Taunay, M. Fishteyn, X. Liu, S. Chandrasekhar, M. Yan, J. Fini, E. Monberg, and F. Dimarcello, "Space-, wavelength-, polarization-division multiplexed transmission of

56 Tb/s over a 76.8 km seven-core fiber," in *Optical Fiber Communication Conf.*, Los Angeles, CA, 2011, paper PDPB7.

[13] S. Chandrasekhar, A. H. Gnauck, X. Liu, P. J. Winzer, Y. Pan, E. Burrows, T. F. Taunay, B. Zhu, M. Fishteyn, M. F. Yan, J. M. Fini, E. Monberg, and F. Dimarcello, "WDM/SDM transmission of 10×128 Gb/s PDM-QPSK over 2688 km 7-core fiber with a per-fiber net aggregate spectral-efficiency distance product of 40,320 km b/s/Hz," *Opt. Express*, vol. 20, no. 2, pp. 706–711, 2012.

[14] J. Sakaguchi, B. Puttnam, W. Klaus, Y. Awaji, N. Wada, A. Kanno, T. Kawanishi, K. Imamura, H. Inaba, K. Mukasa, R. Sugizaki, T. Kobayashi, and M. Watanabe, "19-core fiber transmission of $19 \times 100 \times 172$ Gb/s SDM-WDM-PDM-QPSK signals at 305 Tb/s," in *Nat. Fiber Optic Engineers Conf.*, Los Angeles, CA, 2012, paper PDP5C-1.

[15] S. Randel, R. Ryf, A. Gnauck, M. Mestre, C. Schmidt, R. Essiambre, P. Winzer, R. Delbue, P. Pupalaikis, A. Sureka, Y. Sun, X. Jiang, and R. Lingle, "Mode-multiplexed 6×20 GBd QPSK transmission over 1200 km DGD-compensated few-mode fiber," in *Nat. Fiber Optic Engineers Conf.*, Los Angeles, CA, 2012, paper PDP5C-5.

[16] E. Ip, N. Bai, Y.-K. Huang, E. Mateo, F. Yaman, M.-J. Li, S. Bickham, S. Ten, J. Linares, C. Montero, V. Moreno, X. Prieto, Y. Luo, G.-D. Peng, G. Li, and T. Wang, "6×6 MIMO transmission over 50+25+10 km heterogeneous spans of few-mode fiber with inline erbium-doped fiber amplifier," in *Optical Fiber Communication Conf.*, Los Angeles, CA, 2012, paper OTu2C-4.

[17] S. Jansen, I. Morita, and H. Tanaka, "10×121.9-Gb/s PDM-OFDM transmission with 2-b/s/Hz spectral efficiency over 1,000 km of SSMF," in *Optical Fiber Communication Conf.*, San Diego, CA, 2008, paper PDP2.

[18] S. L. Jansen, I. Morita, and H. Tanaka, "16×52.5-Gb/s, 50-GHz spaced, POLMUX-CO-OFDM transmission over 4,160 km of SSMF enabled by MIMO processing," in *33rd European Conf. and Exhibition of Optical Communication*, 2007, paper PD1.3.

[19] M. Greenberg, M. Nazarathy, and M. Orenstein, "Data parallelization by optical MIMO transmission over multimode fiber with intermodal coupling," *J. Lightwave Technol.*, vol. 25, no. 6, pp. 1503–1514, 2007.

[20] K. Balemarthy and S. Ralph, "MIMO processing of multimode fiber links," in *19th Annu. Meeting of the IEEE Lasers and Electro-Optics Society (LEOS)*, Oct. 2006, pp. 639–640.

[21] K. Appaiah, S. Vishwanath, and S. R. Bank, "Advanced modulation and multiple-input multiple-output for multimode fiber links," *IEEE Photon. Technol. Lett.*, vol. 23, no. 20, pp. 1424–1426, 2011.

[22] B. Thomsen, "MIMO enabled 40 Gb/s transmission using mode division multiplexing in multimode fiber," in *Optical Fiber Communication Conf. (OFC)*, 2010, paper OThM6.

[23] S. Schöllmann and W. Rosenkranz, "Experimental equalization of crosstalk in a 2×2 MIMO system based on mode group diversity multiplexing in MMF systems @ 10.7 Gb/s," in *33rd European Conf. and Exibition of Optical Communication (ECOC)*, 2007, pp. 1–2.

[24] L. Raddatz, I. White, D. Cunningham, and M. Nowell, "An experimental and theoretical study of the offset launch technique for the enhancement of the bandwidth of multimode fiber links," *J. Lightwave Technol.*, vol. 16, no. 3, pp. 324–331, 1998.

[25] Y. Wang, Y. Shao, and N. Chi, "Multiple-inputs multiple-outputs combining center launch and ring launch for high-speed transmission in multimode fiber links," in *Future Wireless Networks and Information Systems*. Springer, 2012, pp. 353–360.

[26] B. Franz, D. Suikat, R. Dischler, F. Buchali, and H. Buelow, "High speed OFDM data transmission over 5 km GI-multimode fiber using spatial multiplexing with 2×4 MIMO processing," in *36th European Conf. and Exhibition on Optical Communication (ECOC)*, 2010, pp. 1–3.

[27] C. Tsekrekos, A. Martinez, F. Huijskens, and A. Koonen, "Design considerations for a transparent mode group diversity multiplexing link," *IEEE Photon. Technol. Lett.*, vol. 18, no. 22, pp. 2359–2361, 2006.

[28] R. Vaze and H. Ganapathy, "Sub-modularity and antenna selection in MIMO systems," *IEEE Commun. Lett.*, vol. 16, no. 9, pp. 1446–1449, Sept. 2012.

[29] G. Herskowitz, H. Kobrinski, and U. Levy, "Optical power distribution in multimode fibers with angular-dependent mode coupling," *J. Lightwave Technol.*, vol. 1, no. 4, pp. 548–554, 1983.

[30] D. Keck, "Spatial and temporal power transfer measurements on a low-loss optical waveguide," *Appl. Opt.*, vol. 13, no. 8, pp. 1882–1888, 1974.

[31] W. Shieh and I. Djordjevic, *OFDM for Optical Communications*. Academic, 2009.

[32] J. Armstrong, "OFDM for optical communications," *J. Lightwave Technol.*, vol. 27, no. 3, pp. 189–204, 2009.

[33] S. Randel, R. Ryf, A. Sierra, P. J. Winzer, A. H. Gnauck, C. A. Bolle, R.-J. Essiambre, D. W. Peckham, A. McCurdy, and R. Lingle, "6×56 Gb/s mode-division multiplexed transmission over 33 km few-mode fiber enabled by 6×6 MIMO equalization," *Opt. Express*, vol. 19, no. 17, pp. 16697–16707, 2011.

[34] M. Blau and D. M. Marom, "Optimization of spatial aperture-sampled mode multiplexer for a three-mode fiber," *IEEE Photon. Technol. Lett.*, vol. 24, no. 23, pp. 2101–2104, 2012.

[35] S. G. Wilson, M. Brandt-Pearce, Q. Cao, and J. H. Leveque, "Free-space optical MIMO transmission with Q-ary PPM," *IEEE Trans. Commun.*, vol. 53, no. 8, pp. 1402–1412, 2005.

[36] H. Bulow, "Optical-mode demultiplexing by optical MIMO filtering of spatial samples," *IEEE Photon. Technol. Lett.*, vol. 24, no. 12, pp. 1045–1047, 2012.

[37] D. Marcuse, *Light Transmission Optics*. New York: Van Nostrand Reinhold, 1982.

[38] E. Zeeb, B. Moller, C. Reiner, M. Ries, T. Hackbarth, and K. Ebeling, "Planar proton implanted VCSEL's and fiber-coupled 2-D VCSEL arrays," *IEEE J. Sel. Top. Quantum Electron.*, vol. 1, no. 2, pp. 616–623, 1995.

[39] R. A. Panicker, J. M. Kahn, and S. P. Boyd, "Compensation of multimode fiber dispersion using adaptive optics via convex optimization," *J. Lightwave Technol.*, vol. 26, no. 10, pp. 1295–1303, 2008.

[40] C. Tsekrekos, M. de Boer, A. Martinez, F. Willems, and A. Koonen, "Temporal stability of a transparent mode group diversity multiplexing link," *IEEE Photon. Technol. Lett.*, vol. 18, no. 23, pp. 2484–2486, 2006.

[41] K. Appaiah, S. Vishwanath, and S. R. Bank, "Vector intensity-modulation and channel state feedback for multimode fiber optic links," *IEEE Trans. Commun.*, vol. 61, no. 7, pp. 2958–2969, 2013.

[42] E. Telatar, "Capacity of multi-antenna Gaussian channels," *Eur. Trans. Telecommun.*, vol. 10, no. 6, pp. 585–595, 1999.

[43] K.-P. Ho and J. M. Kahn, "Mode-dependent loss and gain: Statistics and effect on mode-division multiplexing," *Opt. Express*, vol. 19, no. 17, pp. 16612–16635, 2011.

[44] G. Nemhauser, L. Wolsey, and M. Fisher, "An analysis of approximations for maximizing submodular set functions I," *Math. Program.*, vol. 14, no. 1, pp. 265–294, 1978.

[45] K. Appaiah, S. Zisman, S. Vishwanath, and S. R. Bank, "Analysis of laser and detector placement in MIMO multimode optical fiber systems," in *IEEE Int. Conf. on Communications (ICC)*, June 2012, pp. 2972–2976.

[46] U. Feige and J. Vondrak, "Approximation algorithms for allocation problems: Improving the factor of 1-1/e," in *47th Annu. IEEE Symp. on Foundations of Computer Science (FOCS)*, 2006, pp. 667–676.

[47] S. Schöllmann, S. Soneff, and W. Rosenkranz, "10.7 Gb/s over 300 m GI-MMF using a 2×2 MIMO system based on mode group diversity multiplexing," in *Optical Fiber Communication Conf.*, Anaheim, CA, 2007, paper OTuL2.

[48] L. Tang and D. Miller, "Metallic nanodevices for chip-scale optical interconnects," *J. Nanophoton.*, vol. 3, no. 1, 030302, 2009.

[49] K. Appaiah, R. Salas, S. Vishwanath, and S. R. Bank, "Enhancing data rates in graded-index multimode fibers with offset coupling and multiplexing," in *Optical Fiber Communication Conf.*, Anaheim, CA, 2013.

[50] P. J. Winzer and G. J. Foschini, "MIMO capacities and outage probabilities in spatially multiplexed optical transport systems," *Opt. Express*, vol. 19, no. 17, pp. 16680–16696, 2011.

[51] P. Winzer and G. J. Foschini, "Outage calculations for spatially multiplexed fiber links," in *Optical Fiber Communication Conf.*, Los Angeles, CA, 2011, paper OThO5.

[52] A. Goldsmith, *Wireless Communications*. Cambridge University, 2005.

[53] T. Cormen, C. Leiserson, R. Rivest, and C. Stein, *Introduction to Algorithms*. MIT, 2001.

[54] S. Schollmann and W. Rosenkranz, "Experimental investigations of mode coupling as limiting effect using mode group diversity multiplexing on GI-MMF," in *European Conf. on Optical Communications (ECOC)*, 2006, pp. 1–2.

[55] Y. Li, T. Wang, H. Kosaka, S. Kawai, and K. Kasahara, "Fiber-image-guide-based bit-parallel optical interconnects," *Appl. Opt.*, vol. 35, no. 35, pp. 6920–6933, 1996.

[56] R. Ryf, M. A. Mestre, A. Gnauck, S. Randel, C. Schmidt, R. Essiambre, P. Winzer, R. Delbue, P. Pupalaikis, A. Sureka, Y. Sun, X. Jiang, D. W. Peckham, A. McCurdy, and R. Lingle, Jr., "Low-loss mode coupler for mode-multiplexed transmission in few-mode fiber," in *Nat. Fiber Optic Engineers Conf.*, Los Angeles, CA, 2012, paper PDP5B-5.

[57] N. K. Fontaine, R. Ryf, S. G. Leon-Saval, and J. Bland-Hawthorn, "Evaluation of photonic lanterns for lossless mode-multiplexing," in *European Conf. and Exhibition on Optical Communication*, Amsterdam, The Netherlands, 2012, paper Th-2.

[58] L. Windover, J. Simon, S. Rosenau, K. Giboney, G. Flower, L. Mirkarimi, A. Grot, B. Law, C.-K. Lin, A. Tandon, R. Gruhlke, H. Xia, G. Rankin, M. Tan, and D. Dolfi, "Parallel-optical interconnects >100 Gb/s," *J. Lightwave Technol.*, vol. 22, no. 9, pp. 2055–2063, 2004.

[59] J. Simon, L. Windover, S. Rosenau, K. Giboney, B. Law, G. Flower, L. Mirkarimi, A. Grot, C.-K. Lin, A. Tandon, G. Rankin, R. Gruhlke, and D. Dolfi, "Parallel optical interconnect at 10 Gb/s per channel," in *Proc. of 54th Electronic Components and Technology Conf.*, vol. 1, 2004, pp. 1016–1023.